Multielectrode electroencephalogram power spectra: Theory and application to approximate correction of volume conduction effects

J. A. Henderson,[1] A. J. K. Phillips,[1,2] and P. A. Robinson[1,2]
[1]*School of Physics, University of Sydney, New South Wales 2006, Australia*
[2]*Brain Dynamics Center, Westmead Millenium Institute, Westmead Hospital and Western Clinical School of The University of Sydney, Westmead, New South Wales 2145, Australia*
(Received 14 November 2005; published 31 May 2006)

Using a physiologically based model of brain activity, electroencephalogram (EEG) power spectra are calculated for signals derived from general linear combinations of voltages from multiple electrodes, with and without filtering by volume conduction. Two simple methods of combining scalp measurements to estimate unfiltered EEG power spectra are then proposed and their accuracy and robustness are explored, using the model predictions as an illustration. It is found that these methods, including a case that uses just three electrodes, enable improved estimation of the underlying spectrum relative to each of several widely used combinations alone.

DOI: 10.1103/PhysRevE.73.051918 PACS number(s): 87.10.+e, 87.19.Nn

I. INTRODUCTION

Electroencephalography is widely used to probe brain electrical activity using weighted linear combinations of voltages recorded from combinations (often called *derivations* in the electrophysiological literature) of scalp electrodes [1–3]. In using the electroencephalogram (EEG), one must contend with attenuation and spatial low-pass filtering of the signal in the cerebrospinal fluid, skull, and scalp due to volume conduction. The latter effect results in loss of spatial resolution [2,3], and removal of high temporal frequencies, which are linked to short spatial scales by a dispersion relation. By combining signals from neighboring electrodes to produce higher order derivations, spatial high-pass characteristics can be introduced to compensate approximately for volume conduction [2–5].

In recent years, physiologically based continuum modeling has had considerable success in reproducing single-electrode spectra and a wide variety of other EEG measures (Refs. [6–8] and references cited therein); however, predictions of spectra for general electrode combinations have not been made using these methods, despite the wide use of such derivations experimentally. Nor have there been detailed explorations of their ability to estimate the unfiltered spectrum at the brain surface from the one filtered by volume conduction and observed at the scalp.

This paper has two tasks, motivated by the above considerations. First, we derive the spectra predicted by our physiologically based model for general weighted electrode combinations (derivations). Second, we explore the issue of estimation of underlying power spectra from filtered ones using the method mentioned in the first paragraph above, and illustrate the results using spectra predicted from the model. The aim here is to provide a simple method to improve on single-electrode, bielectrode, or Laplacian estimates alone, which are often used without further processing in the literature. In Secs. II–IV, equations for power spectra of both filtered and unfiltered electrode combinations are derived. In Sec. V various combinations of voltages and resulting spectra are used to demonstrate the restoration of filtered EEG spectra to approximate those at the cortex.

II. MULTIELECTRODE SPECTRA

EEGs record scalp voltage fluctuations that are approximately proportional to fluctuations in activity ϕ_e in excitatory pyramidal neurons in the cerebral cortex [2]. Leaving aside the constant of proportionality, we can thus write a weighted potential difference ψ_N as a linear combination of the individual signals at N electrodes at locations $\mathbf{R}_j$ relative to a nominal location $\mathbf{r}$ (e.g., the centroid) for the derivation as a whole,

$$\psi_N(\mathbf{r},\mathbf{R}_1,\mathbf{R}_2,\ldots,\mathbf{R}_N,t)=\sum_{i=1}^{N} h_i\phi_e(\mathbf{r}+\mathbf{R}_i,t), \tag{1}$$

where h_i is the weight of the ith electrode voltage. For example, the bielectrode potential difference

$$\psi_2(\mathbf{r},\mathbf{R},t)=\phi_e(\mathbf{r}+\mathbf{R},t)-\phi_e(\mathbf{r},t), \tag{2}$$

is the difference in the signals at $\mathbf{r}+\mathbf{R}$ and $\mathbf{r}$ respectively [1], and approximates (aside from a factor $1/R$) the directional derivative of the cortical excitatory field, with

$$\mathbf{R}\cdot\boldsymbol{\nabla}\phi_e(\mathbf{r},t)\approx\phi_e(\mathbf{r}+\mathbf{R},t)-\phi_e(\mathbf{r},t). \tag{3}$$

A commonly used higher-order derivation is the five-electrode combination, ψ_5. Two important special cases are the *equilateral* case, where the spacing of the four electrodes from the central electrode is constant; and the *orthogonal* case where the electrodes are located along two perpendicular axes. The simplest case is then the *equilateral orthogonal* combination, which is used here. Just as the bielectrode signal is related to the directional derivative by (3), so the equilateral, orthogonal signal is related to the Laplacian by

$$R^2\nabla^2\phi_e(\mathbf{r},t)=R^2\left(\frac{\partial^2}{\partial x^2}+\frac{\partial^2}{\partial y^2}\right)\phi_e(\mathbf{r},t), \tag{4}$$

$$\approx\phi_e(\mathbf{r}+R\hat{\mathbf{x}},t)+\phi_e(\mathbf{r}-R\hat{\mathbf{x}},t)+\phi_e(\mathbf{r}+R\hat{\mathbf{y}},t)+\phi_e(\mathbf{r}-R\hat{\mathbf{y}},t)-4\phi_e(\mathbf{r},t), \tag{5}$$

$$=\psi_5(\mathbf{r},R,t), \tag{6}$$

where carets denote unit vectors.

III. POWER SPECTRA

We now determine the unfiltered EEG power spectra for various combinations of electrodes, focusing on the single-electrode, bielectrode, and and five-electrode derivations [6]. Transfer functions calculated from our physiologically based model of cortex and thalamus [7,9] enable spectra to be calculated.

A. Model of underlying activity

In determining scalp power spectra, the underlying neural function of interest is the excitatory cortical activity in pyramidal cells at position $\mathbf{r}$ and time t, $\phi_e(\mathbf{r},t)$ [2]. We recently developed a physiologically based model of EEG generation that predicts EEG observables from quantities such as corticothalamic connectivities, synaptic strengths, dendritic time constants, neural conduction speeds, and axonal ranges, using a continuum approximation to neural tissue [7]. These predictions have reproduced a variety of EEG phenomena [7]. The details of the model, including further details of its underlying assumptions and parameters, are given Ref. [7], so we do not repeat them here.

The theoretical expression for the transfer function, which relates the EEG amplitude ϕ_e at wave vector $\mathbf{k}$ and angular frequency ω to the input stimuli ϕ_n, is [7]

$$\frac{\phi_e(\mathbf{k},\omega)}{\phi_n(\mathbf{k},\omega)} = \frac{G_{es}L}{1-G_{ei}L}\frac{G_{sn}Le^{i\omega t_0/2}}{1-G_{srs}L^2}\frac{1}{k^2r_e^2+q^2r_e^2}, \tag{7}$$

$$q^2r_e^2 = (1-i\omega/\gamma_e)^2 - \frac{L}{1-G_{ei}L}\left(G_{ee} + \frac{(G_{ese}+G_{esre}L)L}{1-G_{srs}L^2}e^{i\omega t_0}\right), \tag{8}$$

$$L = (1-i\omega/\alpha)^{-1}(1-i\omega/\beta)^{-1}, \tag{9}$$

where extensive analysis of the available literature [7] shows that, in the alert waking state, $t_0 \approx 85$ ms is the time taken for signals to travel from cortex to thalamus and back, $\alpha \approx 83\ \mathrm{s}^{-1}$ and $\beta \approx 800\ \mathrm{s}^{-1}$ are dendritic rate constants, $\gamma_e \approx 116\ \mathrm{s}^{-1}$ is a characteristic damping parameter of cortical signals, $r_e \approx 86$ mm is the characteristic excitatory axonal range, and the gains for transmission of signals between various populations of neurons, are $G_{ee} \approx 6.8$ (excitatory to excitatory connections), $G_{ei} \approx -8.1$ (inhibitory interneurons to excitatory connections), $G_{ese} \approx 4.2$ (corticothalamic feedback via thalamic relay cells), $G_{esre} \approx -3.1$ (corticothalamic feedback via thalamic reticular nucleus and thalamic relay cells), $G_{srs} \approx -0.37$ (intrathalamic feedback) $G_{es} \approx 1.7$ (coupling from thalamic relay nuclei to cortex), and $G_{sn} \approx 0.8$ (coupling from external signals to thalamic relay nuclei). These parameter values are used to illustrate our results below; they will change in other cognitive and arousal states. Also, they are assumed to be spatially constant, which is only a first-order approximation to the real situation, which can be handled by appropriate generalization of the model [10].

B. Single electrode spectrum

Before commencing, we note that the single-electrode spectrum is, strictly speaking, the spectrum expected for measurements of one electrode relative to a remote, quiet reference electrode. In reality, this is not attainable, as the reference electrode cannot be positioned very remotely, and is not noise free. Using the average potential of all the electrodes can provide a good approximation if they are sufficiently numerous [3], and we discuss this point further at the end of Sec. III D.

In modeling the single-electrode power spectrum, we assume input stimuli ϕ_n can be approximated by white noise [7], which we set to unit spectral amplitude without loss of generality. The power spectrum, $P(\mathbf{k},\omega)$ is

$$P(\mathbf{k},\omega) = |\phi_e(\mathbf{k},\omega)|^2, \tag{10}$$

whence the frequency spectrum is obtained by integrating over $\mathbf{k}$. Equation (7) implies

$$|\phi_e(\mathbf{k},\omega)|^2 = \frac{A}{|k^2+q^2|^2}, \tag{11}$$

with

$$A = \frac{1}{r_e^4}\left|\frac{G_{es}L}{1-G_{ei}L}\right|^2\left|\frac{G_{sn}L}{1-G_{srs}L^2}\right|^2. \tag{12}$$

Thus, the single-electrode power spectrum, with no volume conduction effects, is

$$P_\phi(\omega) = A\int\frac{d^2\mathbf{k}}{|k^2+q^2|^2}. \tag{13}$$

Changing to polar coordinates in $\mathbf{k}$ space and decomposing into partial fractions then yields

$$P_\phi(\omega) = \frac{2\pi A}{i\ \mathrm{Im}\ q^2}\int_0^\infty dkk\left(\frac{1}{k^2+q^{*2}} - \frac{1}{k^2+q^2}\right), \tag{14}$$

where q^* is the complex conjugate of q and $\mathrm{Im}\ q^2$ denotes the imaginary part of q^2. This gives

$$P_\phi(\omega) = \frac{\pi A}{2i\ \mathrm{Im}\ q^2}\ln\left(\frac{q^2}{q^{*2}}\right). \tag{15}$$

Writing (15) in terms of $\theta = \mathrm{Arg}(q^2)$ gives

$$P_\phi(\omega) = \frac{\pi A\theta}{\mathrm{Im}\ q^2}, \tag{16}$$

which reproduces earlier results [6].

C. Bielectrode spectrum

We can now treat the bielectrode power spectrum

$$P_{\psi 2}(\mathbf{r},\mathbf{R},\omega) = |\phi_e(\mathbf{r}+\mathbf{R},\omega) - \phi_e(\mathbf{r},\omega)|^2. \tag{17}$$

If the cortex is assumed to be spatially homogeneous, the bielectrode potential depends only on the separation of the electrodes $\mathbf{R}$. The power spectrum is then found by averaging over $\mathbf{r}$:

$$P_{\psi 2}(\mathbf{R},\omega) = \langle P_{\psi 2}(\mathbf{r},\mathbf{R},\omega)\rangle_{\mathbf{r}} \tag{18}$$

$$= 2[P_\phi(\omega) - \mathrm{Re}\ U], \tag{19}$$

with

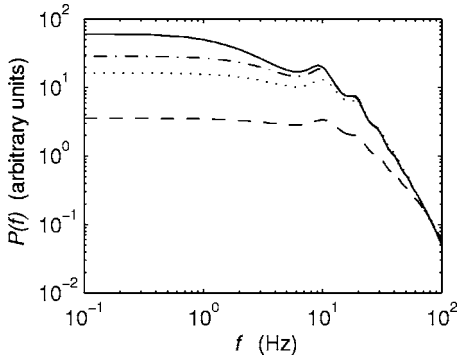

FIG. 1. Effect of electrode separation on unfiltered bielectrode power spectrum. As the separation becomes large the bielectrode power spectrum approaches the solid curve, which represents twice the power spectrum for a single electrode. Separations shown are 0.05 m (dashed), 0.15 m (dotted), and 0.25 m (dashed-dotted).

$$U = \int d^2\mathbf{k} \frac{A}{|k^2 + q^2|^2} e^{i\mathbf{k}\cdot\mathbf{R}}. \tag{20}$$

Simplifying as for the single-electrode case, we find

$$U = \frac{A}{2\,\mathrm{Im}\,q^2} \int_0^{2\pi} d\sigma e^{ikR\cos\sigma} \int_0^{\infty} dk k \left(\frac{1}{k^2 + q^{*2}} - \frac{1}{k^2 + q^2} \right), \tag{21}$$

$$= \frac{\pi A}{\mathrm{Im}\,q^2} \int_0^{\infty} dk k J_0(kR) \left(\frac{1}{k^2 + q^{*2}} - \frac{1}{k^2 + q^2} \right), \tag{22}$$

where J_0 is a Bessel function [11]. A standard result [11] allows the integral to be explicitly expressed in terms of the Macdonald function $K_0(x)$ (a modified Bessel function of the second kind):

$$U = -2\pi A \frac{\mathrm{Im}[K_0(qR)]}{\mathrm{Im}\,q^2}. \tag{23}$$

Finally, substitution into Eq. (19) produces

$$P_{\psi 2}(R,\omega) = \frac{2\pi A}{\mathrm{Im}\,q^2} \{\theta + 2\,\mathrm{Im}[K_0(qR)]\}, \tag{24}$$

in accord with previous work [6].

As the separation R between electrodes becomes large for fixed q, the K_0 term in (24) becomes small and the spectrum approaches the sum of those for the individual electrodes, as shown in Fig. 1. Physically this effect is explained in terms of phase coherence: as the electrodes are moved further apart, the phase difference at any given frequency becomes random. Since our assumed stimulus signal is phase incoherent, the power spectrum approaches twice the single-electrode value.

D. General result, including five-electrode case

From (1), the spectrum for a general derivation is

$$P_{\psi N}(\mathbf{r},\mathbf{R}_1,\ldots,\mathbf{R}_N,\omega) = \left| \sum_{i=1}^{N} h_i \phi_e(\mathbf{r}+\mathbf{R}_i,\omega) \right|^2. \tag{25}$$

Assuming spatial homogeneity, we have

$$P_{\psi N}(\mathbf{R}_1,\ldots,\mathbf{R}_N,\omega) = \langle P_{\psi N}(\mathbf{r},\mathbf{R}_1,\ldots,\mathbf{R}_N,\omega)\rangle_{\mathbf{r}}, \tag{26}$$

$$= \sum_{i=1}^{N} \left(h_i^2 P_\phi(\omega) + 2 \sum_{j=1}^{i-1} h_i h_j \times \int d^2\mathbf{k} \frac{A}{|k^2+q^2|^2} e^{i\mathbf{k}\cdot(\mathbf{R}_i - \mathbf{R}_j)} \right). \tag{27}$$

Recognizing the integral in (27) from (20), we then find

$$P_{\psi N}(\mathbf{R}_1,\ldots,\mathbf{R}_N,\omega) = \frac{\pi A}{\mathrm{Im}\,q^2} \left[\sum_{i=1}^{N} \left(\theta h_i^2 - 4 \sum_{j=1}^{i-1} h_i h_j\, \mathrm{Im}[K_0(q|\mathbf{R}_i - \mathbf{R}_j|)] \right) \right]. \tag{28}$$

The first term in the large square brackets in (28) is the sum of single-electrode contributions, while the second is the sum of bielectrode contributions. The bielectrode case itself has $h_1=1$, $h_2=-1$, $\mathbf{R}_1=\mathbf{R}/2$, and $\mathbf{R}_2=-\mathbf{R}/2$ in (28).

Using (5) and (28) yields the five-electrode spectrum

$$P_{\psi 5}(\mathbf{R},\omega) = \frac{4\pi A}{\mathrm{Im}\,q^2} \mathrm{Im}[5\theta - 2K_0(2qR) - 4K_0(qR\sqrt{2}) + 16K_0(qR)]. \tag{29}$$

Analogously to the bielectrode case, we see that as R becomes large, the K_0 terms become small and the spectrum approaches 20 times that of a single electrode. This factor results from the electrode weightings: there are four electrodes with weightings of 1 and one with a weighting of −4, so the sum of the squares is 20.

Equation (28) can also be used to obtain further insight into how use of the average potential of numerous electrodes as a reference can enable the single-electrode spectrum to be approximated, as noted at the beginning of Sec. III B and in Ref. [3]. If one electrode (the first, without loss of generality) is referenced relative to the average of all N, the weight factors are $h_1=1$ and $h_i=1/N$ for $i>1$. Recognizing that only a fraction of order $1/N$ of electrodes can be close enough to the chosen one to contribute appreciable terms involving the K_0 functions, the contents of the square brackets on the right-hand side of (28) then approach θ in the limit of large N, which leads to (28) reproducing (16) in this limit. Hence, the idealized single-electrode spectrum can be approximated by using the average reference in a sufficiently dense electrode array.

IV. EFFECTS OF VOLUME CONDUCTION

To include the effects of volume conduction through the cerebrospinal fluid, skull, and scalp in spatially filtering the electrode signals we modify (10) to

$$P(\mathbf{k},\omega) = F(k)|\phi_e(\mathbf{k},\omega)|^2, \tag{30}$$

where the low-pass spatial filter function corresponding to volume conduction can be approximated at small to moderate k by $F(k) \approx (1+k^2/k_0^2)^{-1}$ [9]. The parameter k_0 can be estimated from the electrical conductivities and thicknesses of the various tissues overlaying the cortex and from fits of coherence and correlation functions to data, giving $k_0 \approx 29\ \mathrm{m}^{-1}$ which is the value assumed in numerical examples below [9]. This idealization ignores variations in underlying geometry and tissue properties with position on the scalp.

Using methods similar to those in the preceding section, for a general linear combination of electrodes we obtain

$$P_{\psi N}(\omega) = \frac{\pi A}{\mathrm{Im}\, q^2}\left\{\sum_{i=1}^{N}\left[h_i^2\,\mathrm{Im}\left(\frac{\ln(q^2/k_0^2)}{1-q^2/k_0^2}\right) + 4\sum_{j=1}^{i-1} h_i h_j\,\mathrm{Im}\left(\frac{K_0(k_0|\mathbf{R}_i-\mathbf{R}_j|)}{1-q^2/k_0^2} - \frac{K_0(q|\mathbf{R}_i-\mathbf{R}_j|)}{1-q^2/k_0^2}\right)\right]\right\}, \tag{31}$$

where the terms preceded by h_i^2 and $h_i h_j$ are single-electrode and bielectrode contributions, respectively.

For a single electrode the spectrum is given by

$$P_{\phi}(\omega) = \frac{\pi A}{\mathrm{Im}\, q^2}\,\mathrm{Im}\left(\frac{\ln(q^2/k_0^2)}{1-q^2/k_0^2}\right). \tag{32}$$

For a bielectrode one has

$$P_{\psi 2}(\omega) = \frac{2\pi A}{\mathrm{Im}\, q^2}\,\mathrm{Im}\left(\frac{\ln(q^2/k_0^2)}{1-q^2/k_0^2} - \frac{2[K_0(k_0R)-K_0(qR)]}{1-q^2/k_0^2}\right). \tag{33}$$

The five-electrode spectrum is then given by

$$P_{\psi 5}(\omega) = \frac{4\pi A}{\mathrm{Im}\, q^2}\,\mathrm{Im}\left(\frac{1}{(1-q^2/k_0^2)}\{5\ln(q^2/k_0^2) + 2[K_0(2k_0R) - K_0(2qR)] + 4[K_0(k_0R\sqrt{2}) - K_0(qR\sqrt{2})] - 16[K_0(k_0R) - K_0(qR)]\}\right). \tag{34}$$

Once again, as the separation of the electrodes becomes large, the K_0 terms become small and the power spectra above approach multiples of that of the single filtered electrode. Similarly, as $k_0 \to \infty$ the results in this section approach their unfiltered counterparts in Sec. III.

V. CORRECTION FOR VOLUME CONDUCTION EFFECTS ON POWER SPECTRA

Ideally, one would like to estimate the EEG spectrum at a single point on the surface of the brain, rather than the spectrum of a weighted voltage derivation at the scalp. Many authors have developed complex inverse-modeling methods to estimate brain electrical fields from scalp fields, culminating in dura imaging approaches [3] and commercial packages such as LORETA [12]. Others have examined methods for enhancing fine-scale spatial features based on higher-order derivations, and focusing especially on use of the Laplacian [2]. Our approach, which focuses on flattening the volume conduction transfer function, $F(k)$ in (30), complements these by virtue of its simplicity, which makes it easy to implement to obtain useful approximate results.

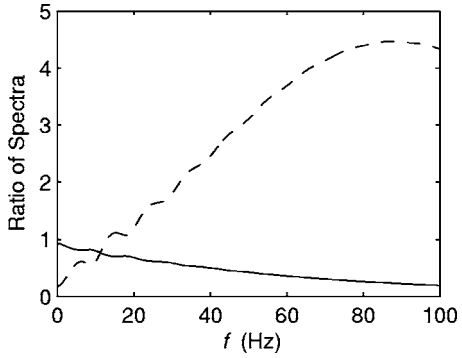

FIG. 2. Ratios of the scalp power spectra for a single electrode (solid) and a five-electrode combination (dashed) to that of a single unfiltered electrode. The ratio for the single scalp electrode decays with frequency, the five-electrode combination increases with frequency.

In order to estimate spectra at the brain surface, we first examine typical scalp spectra for the electrode combinations discussed above and $k_0 = 29\ \mathrm{m}^{-1}$. Figure 2 shows the ratio of the predicted spectrum for a single electrode on the scalp to that for a single electrode on the brain, demonstrating large differences between the two. The relative decay of the scalp spectrum at high frequencies is obvious, with the connection between high spatial and temporal frequencies arising from the wave dispersion relation [2]. At zero frequency, the ratio of the spectra is not exactly unity because wave damping means that the dispersion relation does not correspond to a delta function relationship between ω and $\mathbf{k}$; hence, nonzero k contribute even at $\omega = 0$ and some volume conduction filtering still occurs. In contrast, the five-electrode spectrum shown in Fig. 2 has enhanced power at higher frequencies, despite the effects of filtering, but becomes too small at low frequencies. The ripples in the two curves are another manifestation of the different filtering properties of the two derivations: peaks in the single-electrode spectrum correspond to peaks in the ratio, because weakly damped waves propagate further and thus have higher power and lower k. This also explains the correlation between peaks in the spectrum in Fig. 1 and dips in the five-electrode ratio in Fig. 2: the five-electrode derivation is most sensitive to high k.

The above results suggest that a linear combination of spectra or voltages from a single electrode and a higher-order derivation could yield a power spectrum with little net enhancement or attenuation of any particular frequency, and thus give an improved approximation to the spectrum at the surface of the brain. The electrode weightings can be determined in a number of ways. In each of the following cases, the weighting was determined by adjusting the electrode separation to minimize the largest percentage error found in the composite scalp power spectrum when compared to the

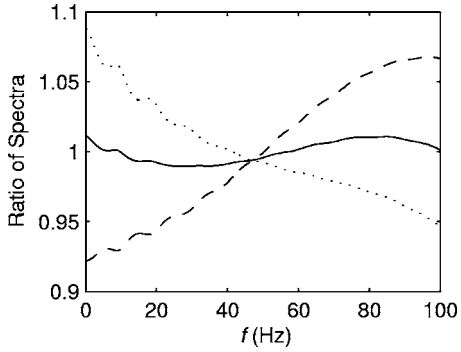

FIG. 3. Ratios of power spectra from (35) to the unfiltered single-electrode spectrum for $R=0.035$ m, and values of a that are optimal (solid, $a=1.61$), 5% lower (dashed), and 5% higher (dotted).

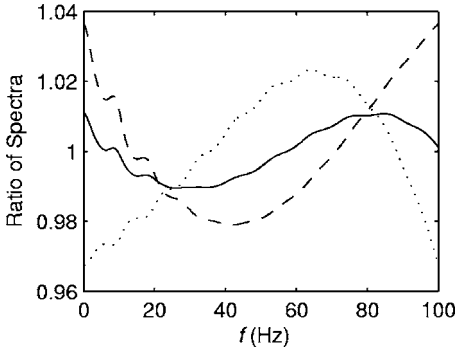

FIG. 4. Ratios of power spectra from Eq. (35) to the unfiltered single-electrode spectrum for optimal electrode separation, $R=0.035$ m (solid, $a=1.61$), 20% lower (dashed, $a=1.45$), and 20% higher (dotted, $a=1.73$). Each curve has its relevant optimized weight factor a.

spectrum for a single electrode on the surface of the brain. Ideally a robust method to tune the weightings for each individual EEG subject would be needed, but use of even a typical value of k_0 will yield better results than either single-electrode, bielectrode, or five-electrode (Laplacian) derivations alone. In this section we illustrate this approach and its sensitivities to electrode spacing and weighting (whose optimal values can only be approximately estimated in experimental situations) using the model spectra and the parameters listed in Sec. III A, which give a good approximation to normal adult waking EEG spectra [7].

A. Linear voltage combination

One method of implementing the ideas above involves changing the weighting of the central electrode in the five-electrode derivation, thereby effectively combining single-electrode and Laplacian components. This gives

$$P_{LV}(R,\omega) = \langle | \phi_e(\mathbf{r}+R\hat{\mathbf{x}},\omega) + \phi_e(\mathbf{r}-R\hat{\mathbf{x}},\omega) + \phi_e(\mathbf{r}+R\hat{\mathbf{y}},\omega) + \phi_e(\mathbf{r}-R\hat{\mathbf{y}},\omega) - a\phi_e(\mathbf{r},\omega)|^2 \rangle_{\mathbf{r}}, \quad (35)$$

for an equilateral orthogonal electrode arrangement, where the constant a is to be determined. In the following figures, we illustrate the use of (35) using model spectra from Sec. III with the parameters in Sec. III A.

Figures 3 and 4 show typical scaled relative power spectra from Eq. (35), spectra are given for optimal values of a (Fig. 3) and R (Fig. 4) and with ±5% and ±20% deviations from optimal values, respectively. In Fig. 3, the separation of electrodes has been held constant to show sensitivity to a. For 1.05 times the optimal value of a, extra weight is placed on the central electrode, skewing the result towards a spectrum more like that for a single electrode, as in Fig. 2. In the $0.95a$ case, the reverse applies and the spectrum is more like a five-electrode spectrum. In Fig. 4, each power spectrum has an optimally tuned a value, demonstrating sensitivity to electrode separation R. In the optimal case there is a small variation in the ratio of spectra with frequency, within 1.1% up to 100 Hz, with ripples associated with spectral peaks, as discussed in connection with Fig. 2 (and which reverses in going from the upper curve to the lower one for the reasons discussed above). A larger value of R reduces the high pass filtering effect, thus requiring a greater weighting on the central electrode. This produces a spectrum more like the five-electrode spectrum at lower frequencies and more like the spectrum for a single electrode at high frequencies. The opposite effect occurs when R is made smaller. The results are summarized in Table I.

A more general approach would be to construct a power spectrum using a signal combination of the form

$$\tilde{P}_{LV} = \sum_{i,j} a_{ij}\phi_i\phi_j^*, \quad (36)$$

where the a_{ij} are weight factors. In principle, these extra free parameters would improve the accuracy of the estimated spectrum. We do not explore this further here as other individual subject effects such as skull nonuniformity are likely to be more important and there would be too many free parameters to determine accurately from the data in any case.

B. Linear power spectrum combination

Another method of approximately correcting the power spectrum for volume-conduction effects is to construct a linear combination of the power spectra of a single-electrode and a higher-order derivation, expressed as

$$P_{LP} = aP_{\phi} + (1-a)P_{\psi N}, \quad (37)$$

where $0 \leqslant a \leqslant 1$ is a constant adjusted to maximize the accuracy of the combination. Here we choose $P_{\psi N}$ to be a three-or five-electrode configuration.

If the $(1+k^2/k_0^2)^{-1}$ filter were exact, it would allow perfect compensation for the filter by using three electrodes arranged to form a right angled isosceles triangle. The signal for this trielectrode derivation is

$$\psi_3(\mathbf{r},R,t) = \phi_e(\mathbf{r}+\hat{\mathbf{x}}R/2-\hat{\mathbf{y}}R/2,t) + \phi_e(\mathbf{r}-\hat{\mathbf{x}}R/2+\hat{\mathbf{y}}R/2,t) - 2\phi_e(\mathbf{r}-\hat{\mathbf{x}}R/2-\hat{\mathbf{y}}R/2,t). \quad (38)$$

The Fourier transform of (38) is

TABLE I. Results of power spectrum estimation using the linear electrode combination and linear combinations of power spectra. Columns three and four show optimal electrode separations R (optimized by varying R from 0.01 m to 0.11 m in steps of 0.005 m for the frequency range listed), and the largest percentage errors encountered in the optimal cases (i.e., when these percentages are minimized by adjusting a and R). Note that the last three lines have an optimal value $R=0.01$ m because this was the smallest value tried; accuracy actually continues to improve slowly as $R\rightarrow 0$ in this case. Conversely, it only degrades slowly with increasing R.

Combination	Freq. Range (Hz)	Optimal R (m)	Accuracy (%)
$\lvert\phi_{+x}+\phi_{-x}+\phi_{+y}+\phi_{-y}-a\phi_0\rvert^2$	0.1–100	0.035	1.09
	0.1–30	0.045	0.18
	30–100	0.035	0.63
$aP_\phi+(1-a)P_{\psi 5}$	0.1–100	0.055	5.88
	0.1–30	0.110	0.90
	30–100	0.045	1.71
$aP_\phi+(1-a)P_{\psi 3}$	0.1–100	0.010	0.57
	0.1–30	0.010	0.18
	30–100	0.010	0.57

$$\psi_3(\mathbf{k},\omega)=(e^{iR(k_y-k_x)/2}+e^{iR(k_x-k_y)/2}-2e^{-iR(k_x+k_y)/2})\phi_e(\mathbf{k},\omega), \tag{39}$$

giving the power spectrum

$$P_{\psi 3}(\mathbf{k},\omega)=\{6+2\cos[R(k_y-k_x)]-4[\cos(Rk_x)+\cos(Rk_y)]\}|\phi_e(\mathbf{k},\omega)|^2. \tag{40}$$

Using the first two terms in the Taylor expansion of the cosine function, we can approximate (40) to give

$$P_{\psi 3}(\omega)=\int d^2\mathbf{k}\frac{(Rk)^2|\phi_e(\mathbf{k},\omega)|^2}{1+k^2/k_0^2}, \tag{41}$$

with the inclusion of the filter function. Combining this result with the single-electrode spectrum, as in (37), gives

$$P_{LP}(\omega)=\int d^2\mathbf{k}\left(\frac{a+(1-a)R^2k^2}{1+k^2/k_0^2}\right)|\phi_e(\mathbf{k},\omega)|^2. \tag{42}$$

If we then choose

$$a=\frac{k_0^2R^2}{k_0^2R^2+1}, \tag{43}$$

we have

$$P_{LP}(\omega)=a\int d^2\mathbf{k}|\phi_e(\mathbf{k},\omega)|^2, \tag{44}$$

which reproduces the unfiltered power spectrum exactly, apart from the constant a. In principle, the value of k_0 could be obtained by requiring that P_{LP} differ only in normalization for two different values of R, but in practice, confounding factors such as nonuniformities and inaccuracies in the approximations made above are likely to prevent this from being feasible.

Due to the approximation made in obtaining Eq. (41) and (44) is only valid for values of R below a limit that depends on the frequency range of interest and values of the parameters in the model. With $R=0.03$ m (not shown) an error of about 5% occurs over the frequency range 0–100 Hz. By including higher order terms and/or higher order derivations the approximation in Eq. (41) might be improved to allow larger electrode separations; however, the additional complexity is not warranted, given the level of individual variation and the confounding factors mentioned in the preceding paragraph.

In the following figures, we illustrate the above method, and its sensitivities to R and a using the model spectra and parameters from Sec. III A. Figure 5 shows four ratios of spectra for a trielectrode combination, where a' is the optimal value, a is given by (43), or where there are ±5% deviations from this value. Even with a deviation from a or a', the resulting spectrum is a good approximation to the unfiltered single-electrode spectrum. In the case with a given exactly by (43), the relative power spectrum falls slowly, since increasing the frequency decreases the accuracy of the approxi-

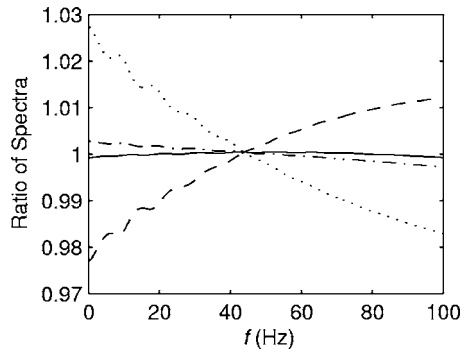

FIG. 5. Ratios of power spectra for an optimized combination of the form $aP_\phi+(1-a)P_{\psi 3}$ to the unfiltered single-electrode spectrum. Electrode separation is 0.01 m. The weighting has an optimal value $a'=0.091$ (solid curve), a value $a=0.090$ given by Eq. (43) (dotted-dashed), and values of $0.95a$ (dashed) and $1.05a$ (dotted).

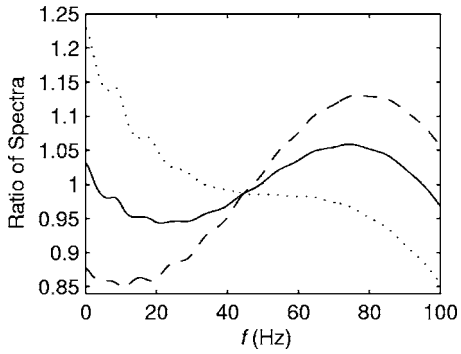

FIG. 6. Ratios of power spectra for a combination $aP_{\phi}+(1-a)P_{\psi 5}$ with $R=0.055$ m to the unfiltered single-electrode spectrum. The weighting a is assumed to be optimal (solid, $a=0.86$), 5% lower (dashed), or 5% higher (dotted).

mation in Eq. (41). The ratio of the spectra is close to, but less than, unity at very low frequencies as there are nonzero k, and as a result there is error in the approximation of Eq. (41). No dependence of separation is shown for the trielectrode as smaller separations will always produce more accurate results.

Figures 6 and 7 show typical scaled relative power spectra from Eq. (37) with $N=5$. Spectra are given for optimal values of a (Fig. 6) and R (Fig. 7) and also with ±5% and ±20% deviations from these values, respectively. In Fig. 6, the separation of electrodes has been held constant to show sensitivity to a. In Fig. 7, each spectrum has an optimal a value, with the spectra showing sensitivity to electrode separation R. The general features are explained as in Sec. V A for the five-electrode linear voltage combination.

Table I summarizes indicative results of power spectrum restoration by the three methods. The trielectrode combination of power spectra provides the best results, as expected from discussion in Sec. V B. This is especially useful as the weight and scaling factor can be predicted with reasonable accuracy from Eq. (43), allowing a simpler practical implementation. The optimal electrode separations are no smaller than those of the high density arrays (64 or more electrodes) that are increasingly used for EEG studies. The exception is

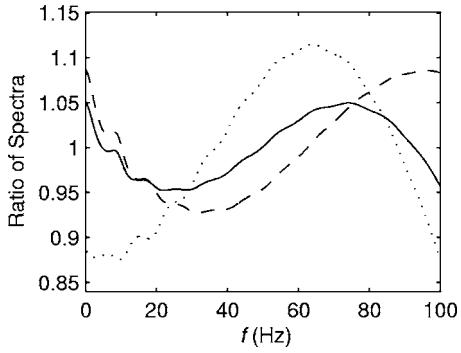

FIG. 7. Ratios of power spectra to the unfiltered single-electrode spectrum for a combination $aP_{\phi}+(1-a)P_{\psi 5}$ with optimal electrode separation, $R=0.055$ m (solid, $a=0.865$), a value 20% lower (dashed, $a=0.810$), and 20% higher (dotted, $a=0.860$). Each curve has an optimized weight factor a.

in the last three lines of the table where the optimum actually occurs at zero separation, but where the accuracy is expected to degrade relatively slowly with R, based on the analysis in Sec. V B.

In all cases the spectrum was most accurately approximated over the range 0–30 Hz, due to the fact that volume conduction filters higher frequencies more heavily, thereby requiring more substantial correction. It is also noted that a larger electrode separation gave a better approximation in this frequency range, but the reverse is true in the 30–100 Hz range. To explain this we consider Eq. (31), where the K_0 terms become small as $|\mathbf{R}_i-\mathbf{R}_j|$ increases, resulting in a spectrum that approaches a multiple of the spectrum for an individual electrode. In the low frequency range this is appropriate because the power spectrum is only slightly affected by volume conduction, so we require only slight high-pass filtering to compensate. However, at high frequencies, the high-frequency part of the spectrum is heavily attenuated by volume conduction, so the high-pass filter needs to be increased by reducing the separation of the electrodes.

VI. SUMMARY

In the first part of this paper we derived physiologically based expressions for both filtered and unfiltered EEG power spectra for a general linear combination of electrode voltages. Explicit expressions for single-, bi-, and five-electrode cases were written down, and limiting cases were explored. As expected, multielectrode spectra generally filter out long-wavelength contributions, emphasizing shorter wavelengths and, hence, higher frequencies. At large electrode separations, multielectrode spectra approach constant multiples of the single-electrode spectrum. We also elucidated how the single-electrode spectrum can be approximated by using the average potential of a sufficiently dense electrode array as the reference.

In the second part of the paper two methods were proposed to estimate unfiltered spectra from scalp spectra, one involving linear combinations of power spectra, and the other using linear combinations of electrode voltages. Both methods use admixtures of high pass filtering to correct for the low-pass filtering that results from volume conduction, in essence flattening the k dependence of the transfer function from brain to scalp.

The results of the above spectral estimation methods were illustrated, and their sensitivity to electrode separation R and weighting a were explored, using spectra predicted from our physiologically based model. Specifically, the method of combining power spectra was implemented using two different electrode combinations, one using five-electrodes and the other using a trielectrode combination. The trielectrode allows a simple analytic calculation of the electrode weights and was found to be very accurate for small electrode separations, although a practical limit is imposed by the accuracy with which voltage differences can be measured at small scales. Sensitivities to the electrode separation and weights were found to be small enough that the power spectrum could be estimated with reasonable accuracy and robustness,

even if R and a are not precisely known. The results should also be fairly independent of brain state, since they correct for volume conduction effects, which do not change with state. Accuracies will, however, change slightly in different states because of their different frequency and wave-number content.

The methods suggested should thus provide a significant improvement on use of single-electrode or Laplacian methods alone in estimating underlying spectra at the brain. This is likely to be of most use in obtaining improved first-order estimates of spectra, which are very often all that is desired in experimental situations. Where more sophisticated analyses are desired, to cope with spatial nonuniformities in parameters, for example, similar ideas may be able to be incorporated into methods such as those discussed by Nunez and Srinivasan [3].

ACKNOWLEDGMENTS

The authors thank C. J. Rennie for his comments on the paper. This work was supported by the Australian Research Council.

[1] E. Niedermeyer, in *Electroencephalography: Basic Principles, Clinical Applications, and Related Fields*, 4th ed., edited by E. Niedermeyer and F. H. Lopes da Silva (Williams and Wilkins, Baltimore, 1999).

[2] P. L. Nunez, *Neocortical Dynamics and Human EEG Rhythms* (Oxford University Press, Oxford, 1995).

[3] P. L. Nunez and R. Srinivasan, *Electric Fields of the Brain: The Neurophysics of EEG*, 2nd ed. (Oxford University Press, Oxford, 2005).

[4] P. L. Nunez, R. Srinivasan, A. F. Westdorp, R. S. Wijesinghe, D. M. Tucker, R. B. Silberstein, and P. J. Cadusch, Electroencephalogr. Clin. Neurophysiol. **103**, 499 (1997).

[5] P. L. Nunez, R. B. Silberstein, Z. P. Shi, M. R. Carpenter, R. Srinivasan, D. M. Tucker, S. M. Doran, P. J. Cadusch, and R. S. Wijesinghe, Electroencephalogr. Clin. Neurophysiol. **110**, 469 (1999).

[6] P. A. Robinson, J. Theor. Biol. **222**, 163 (2003).

[7] P. A. Robinson, C. J. Rennie, D. L. Rowe, and S. C. O'Connor, Hum. Brain Mapp **23**, 53 (2004).

[8] P. A. Robinson, C. J. Rennie, D. L. Rowe, S. C. O'Connor, and E. Gordon, Philos. Trans. R. Soc. London, Ser. B **360**, 1043 (2005).

[9] P. A. Robinson, C. J. Rennie, J. J. Wright, H. Bahramali, E. Gordon, and D. L. Rowe, Phys. Rev. E **63**, 021903 (2000).

[10] S. C. O'Connor and P. A. Robinson, Phys. Rev. E **70**, 011911 (2004).

[11] M. Abramowitz and I. A. Stegun, *Handbook of Mathematical Functions* (Dover, New York, 1970).

[12] R. D. Pascual-Marqui, C. M. Michel, and D. Lehmann, Int. J. Psychophysiol **18**, 49 (1994).